Letter

Pinch points and half-moons in dipolar-octupolar Nd$_2$Hf$_2$O$_7$

A. Samartzis [1,2,*] J. Xu,[1,3] V. K. Anand,[1,4] A. T. M. N. Islam,[1] J. Ollivier,[5] Y. Su [6] and B. Lake [1,2,†]

[1]*Helmholtz-Zentrum Berlin für Materialien und Energie, Hahn-Meitner-Platz 1, D-14109 Berlin, Germany*
[2]*Institut für Festkörperphysik, Technische Universität Berlin, Hardenbergstrasse 36, D-10623 Berlin, Germany*
[3]*Heinz Maier-Leibnitz Zentrum at Lichtenbergstrasse 1, D-85748 Garching, Germany*
[4]*Department of Physics, University of Petroleum and Energy Studies, Dehradun, Uttarakhand 248007, India*
[5]*Institut Laue Langevin, 6 rue Jules Horowitz, BP 156, F-38042 Grenoble, France*
[6]*Jülich Centre for Neutron Science at Heinz Maier-Leibnitz Zentrum, Forschungszentrum Jülich GmbH,
Lichtenbergstr. 1, D-85747 Garching, Germany*

While it is established that the pinch point scattering pattern in spin ice arises from an emergent Coulomb phase associated with a magnetic moment that is divergence free, more complex Hamiltonians can introduce a divergence-full part. If these two parts remain decoupled, they give rise to the coexistence of distinct features. Here, we show that the moment in Nd$_2$Hf$_2$O$_7$ forms a static long-range ordered ground state, a flat, gapped pinch point excitation, and dispersive excitations. These results confirm recent theories which predict that the dispersive modes, which arise from the divergence-full moment, host a pinch point pattern of their own, observed experimentally as "half-moons."

The observation of a "pinch point pattern" in magnetic materials signals the presence of an emergent Coulomb phase where the divergence of the emergent vector field (in this case the magnetization) is zero (divergence free) [1]. The pinch point pattern arises in classical spin-ice materials such as Ho$_2$Ti$_2$O$_7$ [2,3] or Dy$_2$Ti$_2$O$_7$ [4] where the magnetic rare-earth ions which lie on the verticies of a network of corner-share tetrahedra (pyrochlore lattice) are coupled by ferromagnetic (FM) interactions and have strong local Ising anisotropy that forces the spins to point into or out of the center of every tetrahedron. This highly frustrated combination of FM interactions and Ising anisotropy gives rise to the ice rule that states that in the ground state, two spins point into and two spins point out of each tetrahedron (2I2O configuration), leading to a highly degenerate ground state manifold [5]. Excitations from this state (such as three spins pointing into and one spin pointing out of a tetrahedron) are magnetic monopoles [3,4,6]. Quantum spin ice can arise in materials where additional weak terms in the Hamiltonian allow mixing of the ground state manifold to give a spin-liquid state [7,8]. Violations of the ice rule and the divergence-free condition allow monopole creation in the ground state, observed experimentally as a broadening of the pinch points [9].

More complex Hamiltonians can give rise to further changes in the magnetic properties. A particularly interesting phenomenon proposed recently is magnetic moment fragmentation, where the magnetic Hamiltonian contains both divergence-free and divergence-full parts [10]. These sectors can remain decoupled, allowing, for example, for the coexistence of long-range magnetic order in the form of a monopole

crystal (divergence full) alongside a static pinch point pattern (divergence free). Related phenomena were observed in Nd$_2$Zr$_2$O$_7$. Here, the dipolar-octupolar doublet of the Nd^{3+} ion [11,12] gives rise to a Hamiltonian that has both FM and antiferromagnetic (AFM) interactions for different spin components as well as Ising anisotropy. The weak unfrustrated AFM term gives rise to long-range magnetic order with the all-in/all-out (AIAO) configuration where all the spins point into or all out of each tetrahedra (divergence full) [12,13]. In contrast the FM term gives rise to a pinch point pattern which is dynamic and forms a divergence-free excitation [14,15]. Application of a magnetic field was found to induce further exotic behaviors [16–18].

Here, we investigate another feature related to moment fragmentation, namely "half-moons." These are rings observed in inelastic neutron scattering where the intensity is strongly modulated around the ring, rather than the uniform intensity distribution typical of conventional magnetic excitations such as spin waves. While they have occasionally been glimpsed in experiments [14,16,19,20] as well as in numerical simulations [21–26], they were not studied systematically and their significance was not explained. Very recently the half-moons were investigated by two theoretical groups who showed that they arise from a divergence-full moment and signal proximity to an emergent Coulomb phase [27,28].

In this Letter we study the pyrochlore Nd$_2$Hf$_2$O$_7$ using neutron scattering measurements and show that it hosts half-moons. Previous investigations of Nd$_2$Hf$_2$O$_7$ reveal that the crystal electric field surrounding the magnetic Nd^{3+} ion results in a Kramers doublet ground state, well isolated from the first excited state [29]. The ground state wave function of the Nd^{3+} ion is of dipolar-octupolar nature with Ising anisotropy and the g tensor was found to be $g_{zz} \approx 5.1$, $g_{xx} = g_{yy} = 0$ within the pseudo-spin-1/2 model where z is the local [1,1,1]

*alexandros.samartzis@helmholtz-berlin.de
†bella.lake@helmholtz-berlin.de

axis pointing towards the center of each tetrahedron [29]. $Nd_2Hf_2O_7$ orders below $T_N = 0.55$ K in the AIAO magnetic structure [30], indicating the presence of an AFM interaction. The ordered moment at $T = 0.1$ K is $m = 0.62\mu_B$ [30], which is strongly reduced compared to the effective moment of the ground state wave function of $2.45\mu_B$, indicating the presence of quantum fluctuations as also inferred from muon spin relaxation measurements [29]. $Nd_2Hf_2O_7$ was also found to demonstrate an inverted magnetic hysteresis loop for magnetic fields along the [1,1,1] and [0,0,1] directions [31].

In this present Letter we find that AIAO antiferromagnetic long-range order of $Nd_2Hf_2O_7$ coexists with a dynamical pinch point pattern that takes the form of a flat gapped mode. In addition there are higher energy dispersive modes which give rise to half-moon features. We perform a detailed examination of these dispersive modes and the associated half-moons and achieve excellent agreement between our data and simulations. Our results confirm the recent theories [27,28] that predict that these modes, which arise from the divergence-full part of the moment, also host a pinch point pattern of their own.

Neutron scattering was performed on a large single crystal of $Nd_2Hf_2O_7$ of mass ≈ 6 g oriented to access the $[H, H, L]$ reciprocal lattice plane. Inelastic neutron scattering (INS) was measured at the Institut Laue Langevin, France, on the direct geometry, time-of-flight spectrometer IN5 [32], with neutrons of wavelength 6 Å and energy resolution 0.041 meV. ω scans were measured far below $T_N = 0.55$ K at 40 mK, just above T_N at 600 mK as well as at 25 K which was used to estimate the nonmagnetic background. The data were background subtracted, normalized, and analyzed using the HORACE software [33] (see Supplemental Material [34]). Polarized neutron diffraction (PND) was measured using DNS at the Maier-Leibniz Zentrum, Germany [35] with neutrons of wavelength 4.2 Å. The neutrons were polarized along the (vertical) Z direction and both spin-flip (ZSF) and non-spin-flip (ZNSF) channels were measured for ω scans at 88 mK, 600 mK, and 25 K.

Figure 1(c) presents the PND data below T_N at 88 mK. The data show a pinch point pattern coexisting with the magnetic Bragg peaks of the AIAO order at (2,2,0), (1,1,3), and $(-1, -1, 3)$. The pinch points, expected at (0,0,2), (1,1,1), and (2,2,2), are not sharp, revealing that the ice rule is not perfectly obeyed due to the presence of additional interactions beside the Ising term between the Nd^{3+} ions. The data give the magnetic signal integrated over energy, and to resolve the energy scales of the various features we turn to the INS data. Figure 1(e) shows a cut through the INS data plotted as a function of energy. Below T_N at 40 mK, a peak is observed at $E \approx 0.1$ meV. A second broad peak occurs at ≈ 0.28 meV, while by 0.4 meV the scattering approaches the nonmagnetic background provided by the 25-K data.

Wave-vector maps in the $[H, H, L]$ plane of the INS data at 40 mK are shown in Fig. 2. For $0.06 < E < 0.1$ meV [Fig. 2(a)] which corresponds to the first peak in Fig. 1(e), a clear pinch point pattern is found where the pinch points appear sharper than those observed in the PND data [Fig. 1(c)]. At energies below this peak, the pinch point pattern has disappeared. These results show that the pinch point pattern is from a dynamic gapped mode well separated in energy from the
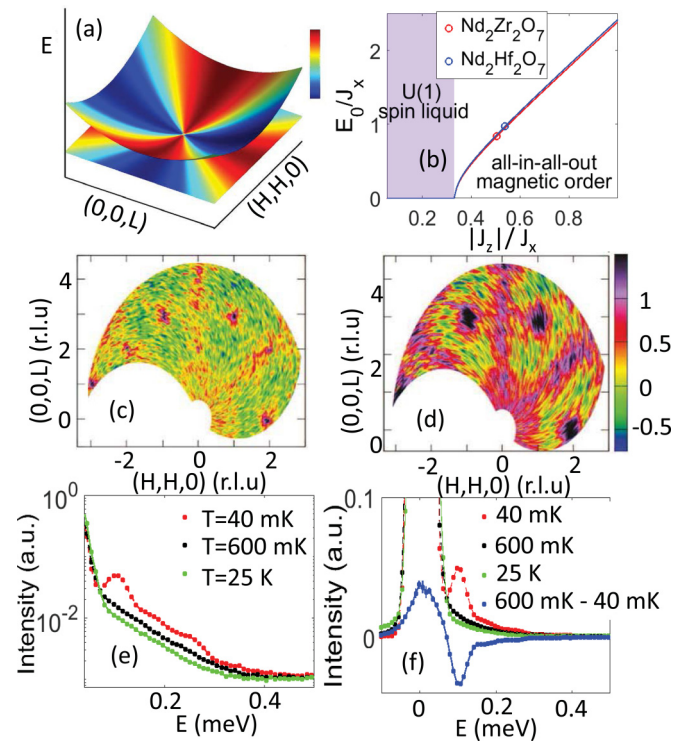

FIG. 1. (a) Theoretical spectrum as a function of wave vector in the $[H, H, L]$ plane and energy, showing the flat pinch point mode and the dispersive half-moon mode which touch at the pinch points; the colors indicate the intensity of the dynamic structure factor [27]. (b) Phase diagram of the XYZ Hamiltonian showing the gap of the pinch point mode, $E_0 = \sqrt{(3|\tilde{J}_{\tilde{z}}| - \tilde{J}_{\tilde{x}})(3|\tilde{J}_{\tilde{z}}| - \tilde{J}_{\tilde{y}})}$, as a function of $|\tilde{J}_{\tilde{z}}|/\tilde{J}_{\tilde{x}}$ [36]. The circles locate $Nd_2Hf_2O_7$ and $Nd_2Zr_2O_7$. (c), (d) $[H, H, L]$ wave-vector map of the background-subtracted Z-spin-flip PND measured at (c) 88 mK and (d) 600 mK. The presence of signal at the nuclear Bragg peaks (2,2,2) and (0,0,2) is due to the subtraction of two large numbers. (e) INS spectra at $T = 40$ mK, $T = 600$ mK, and $T = 25$ K integrated over a large wave-vector range ($[H, H, L]$: $-1 < H < 1.5$; $0.5 < L < 2.5$) and plotted on a log scale as a function of energy, with no background subtraction or normalization. (f) The same data on a linear scale including a plot of the difference between the 600- and 40-mK data sets; the Bragg peaks were removed before the subtraction.

AIAO ground state. Energy versus wave-vector slices through the INS data at $T = 40$ mK are displayed in Fig. 3 for several directions. The most striking feature is the sharp, gapped, dispersionless mode lying at an energy of $E_0 = 0.094$ meV. This is the pinch point mode observed in the constant energy cut at $0.06 < E < 0.1$ meV [Fig. 2(b)]. At higher energies there are sharp dispersive modes.

These measurements reveal the unusual coexistence in $Nd_2Hf_2O_7$ of a long-range AIAO magnetically ordered ground state with a dynamical pinch point pattern associated with the 2I2O spin fluctuations of an emergent Coulomb phase. The divergence-full and divergence-free parts of the magnetic moment are responsible for these two phenomena, respectively. Similar magnetic behavior was observed in the related compound $Nd_2Hf_2O_7$ [14,15].
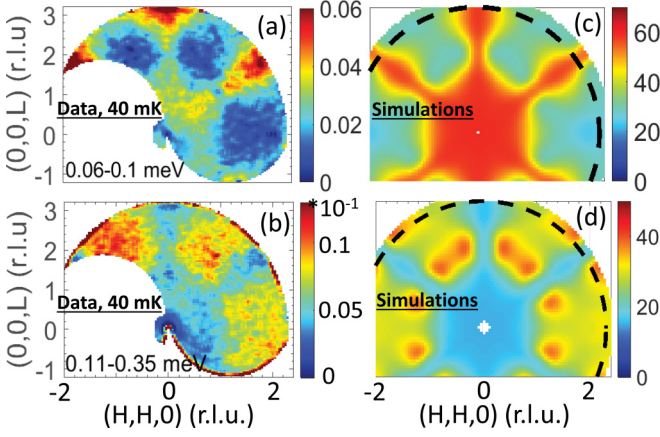
FIG. 2. Comparison of the experimental and theoretical spectrum of $Nd_2Hf_2O_7$ in the $[H, H, L]$ plane. (a) and (b) show the INS data at 40 mK integrated over the flat ($0.06 < E < 0.1$ meV) and dispersive ($0.11 < E < 0.35$ meV) modes, respectively. The data were also integrated over the out-of-plane wave vector $[K, -K, 0]$ by $K = \pm 0.1$ r.l.u. and they were normalized and the background was subtracted [34]. (c) and (d) show the corresponding neutron scattering structure factor simulated for the Hamiltonian H_{XYZ}^{DO} [Eq. (1)] using linear spin-wave theory [34] integrated over the same energy and wave-vector ranges.

Here, we use the XYZ Hamiltonian, proposed for $Nd_2Zr_2O_7$ [36,37] to describe $Nd_2Hf_2O_7$ and obtain the interactions,

$$H_{XYZ}^{DO} = \sum_{\langle ij \rangle} \widetilde{J}_{\widetilde{x}} \widetilde{\tau}_i^{\widetilde{x}} \widetilde{\tau}_j^{\widetilde{x}} + \widetilde{J}_{\widetilde{y}} \widetilde{\tau}_i^{\widetilde{y}} \widetilde{\tau}_j^{\widetilde{y}} + \widetilde{J}_{\widetilde{z}} \widetilde{\tau}_i^{\widetilde{z}} \widetilde{\tau}_j^{\widetilde{z}}, \tag{1}$$

where $\widetilde{\tau}_i^{\widetilde{\alpha}}$ is the $\widetilde{\alpha}$ component of the ith pseudospin-1/2 operator and $\widetilde{J}_{\widetilde{\alpha}}$ is the exchange interaction between the $\widetilde{\alpha}$ components of nearest-neighbor spins. A rotated local coordinate system is used where $\widetilde{z}$ is rotated by an angle θ from the local $(1,1,1)$ axis [34,38].

The Hamiltonian was determined by fitting linear spin-wave theory [39] to the INS data [34]. The results presented on the left-hand side of Figs. 2 and 3 agree excellently with the data. The fits yielded $\widetilde{J}_{\widetilde{x}} = 0.106(5)$ meV, $\widetilde{J}_{\widetilde{y}} = 0.008(5)$ meV, $\widetilde{J}_{\widetilde{z}} = -0.057(4)$ meV, while $\theta \approx 72.5°$ was obtained from the Curie-Weiss temperature [34]. $\widetilde{J}_{\widetilde{x}}$ is ferromagnetic and would, on its own, give rise to a classical, highly degenerate, "rotated spin-ice" ground state with a 2I2O spin configuration characterized by a pinch point pattern at zero energy transfer. The addition of a weak antiferromagnetic $\widetilde{J}_{\widetilde{z}}$ introduces quantum fluctuations which mix the extensive ground state manifold to give a $U(1)$ spin liquid [36]. For $|\widetilde{J}_{\widetilde{z}}| > \widetilde{J}_{\widetilde{x}}/3$, a long-range AIAO ordered ground state is induced, and the pinch point becomes dynamic and gapped as is the case for $Nd_2Hf_2O_7$. Figure 1(b) shows the phase diagram with the gap plotted as a function of $|\widetilde{J}_{\widetilde{z}}|$ and the location of $Nd_2Hf_2O_7$ proximate to the $U(1)$ spin liquid.

The origins of this apparent magnetic moment fragmentation for the XYZ Hamiltonian were investigated by O. Benton and found to be a consequence of the dipolar-octupolar nature of the Kramers doublet ground state of Nd^{3+} and the equations of motion of the magnetic degrees of freedom
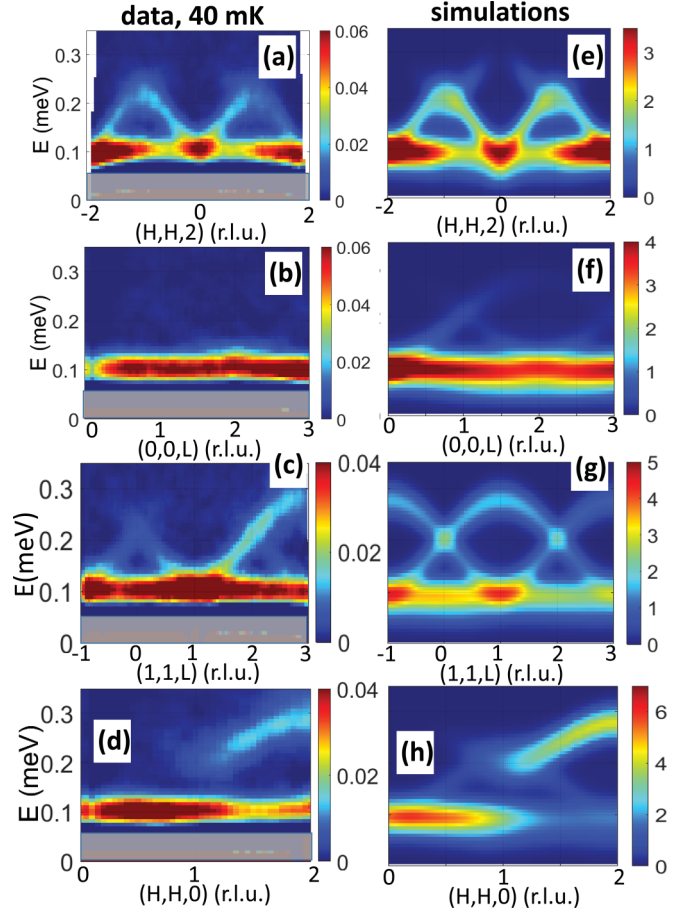

FIG. 3. Energy-wave-vector maps comparing the experimental and theoretical spectrum of $Nd_2Hf_2O_7$. (a)–(d) show the INS measurement at 40 mK along various reciprocal space directions. The data were integrated over the out-of-plane and the in-plane wave vectors perpendicular to the slice by ± 0.2 r.l.u., and were normalized and background subtracted [34]. The data below 0.06 meV (shaded region) are unreliable due to background oversubtraction. (e)–(h) show the corresponding neutron scattering structure factor simulated for H_{XYZ}^{DO} [Eq. (1)] using linear spin-wave theory [34] for the same wave-vector integrations.

[36]. He proposed that the AIAO magnetic order (due to $\widetilde{\tau}_i^{\widetilde{z}}$) is entirely divergence full, while the dynamics (due to $\widetilde{\tau}_i^{\widetilde{x}}$ and $\widetilde{\tau}_i^{\widetilde{y}}$) completely decouple into a divergence-free part responsible for the flat pinch point mode and a divergence-full part which gives rise to the dispersive modes at higher energies.

Because of its proximity to the $U(1)$ quantum spin-liquid state we would expect $Nd_2Hf_2O_7$ to show signatures of this spin liquid just above $T_N \approx 0.55$ K when the AIAO magnetic order is lost. Figure 1(d) shows the PND measurement at $T = 0.6$ K $(>T_N)$, where the pinch point pattern is enhanced compared to $T = 0.088$ K [Fig. 1(c)] and the pinch points are broadened. In addition, the AIAO Bragg peaks at $(2,2,0)$, $(3,1,1)$, and $(3,-1,-1)$ have been replaced by broad features. Figure 1(e) shows an energy cut through the INS data at 0.6 K. The pinch point mode at 0.094 meV, as well as the 0.28 meV peak found at $T = 0.04$ K, have been replaced by broad magnetic signal peaked at the elastic energy. This

is shown clearly in Fig. 1(f) where the difference is taken between the cuts at 0.6 and 0.04 K, revealing that the peak found at 0.094 meV below T_N is replaced by a peak at ≈ 0 meV above T_N. Similar results were observed for $Nd_2Zr_2O_7$ where above T_N the pinch point was found at elastic energies. Here, the transition was attributed to a Higgs transition where the emergent gauge field of the Coulomb phase above T_N becomes gapped by the condensation of emergent gauge charges or monopoles into the ground state below T_N [40]. Another study however found more complex behavior with the coexistence of inelastic and elastic pinch point patterns above T_N [41].

We now return to low temperatures and take a closer look at the high energy dispersive excitations ($E > 0.11$ meV) which show several unconventional features. First, these modes have maximum energy at the wave vectors of the magnetic Bragg peaks [(1,1,2) and (2,2,0)] rather than being minimum there, as is usually the case for an ordered system (Figs. 2 and 3). Instead their energy minima occur at the wave vectors of the pinch points (0,0,2), (1,1,1), and (2,2,2) where they touch the flat gapped mode. Furthermore, an integration of the dispersive modes over energy ($0.11 < E < 0.35$ meV) shows that they have maximum intensity close to these pinch point wave vectors, but curiously the intensity distribution is opposite to that of the flat pinch point mode (Fig. 2). The flat mode shows the traditional pinch point pattern with a streak of intensity along the radial wave vectors [Fig. 2(a)], but the dispersive modes have the opposite intensity distribution with a signal concentrated at the transverse wave vectors [Fig. 2(b)]. Finally, wave-vector maps for narrow energy integration ranges, just above the minima of the dispersive modes, do not show the rings typically observed when slicing through cone-shaped dispersions; instead, "split-ring" or "half-moon" features surrounding the pinch point wave vectors are observed with opposite intensity distribution to the flat mode (Fig. 4). By taking a series of energy slices we show that the half-moons disperse away from the pinch point with increasing energy but never become complete rings. Their behavior is well captured by the spin-wave simulations which show good agreement with the data in Fig. 4.

Half-moons have been glimpsed occasionally in INS data from pyrochlore magnets such as $Tb_2Ti_2O_7$ [19,20] and $Nd_2Zr_2O_7$ [14,16] as well as in numerical simulations of kagome- and pyrochlore-related magnets [21–26], however, a systematic experimental investigation has not been performed, nor has an explanation for their existence been given until recently. Mizoguchi *et al.* [28] showed that half-moons can be interpreted as shadows of pinch points, signaling proximity to a Coulomb phase. From a real-space perspective, they reflect the formation of magnetic clusters involving short-range correlation of conserved spin, e.g., due to further neighbor interactions in Heisenberg magnets. Yan *et al.* [27] used a Helmholtz decomposition to make the connection between traditional pinch points (satisfying the divergence-free condition) and half-moons (satisfying the divergence-full condition) proving they originate from the same, proximate, $U(1)$ gauge symmetry. They further showed that half-moons themselves arise from a rotated pinch point pattern that is oriented perpendicular to the conventional pinch point pattern and exists on a cone-shaped dispersing mode centered at the
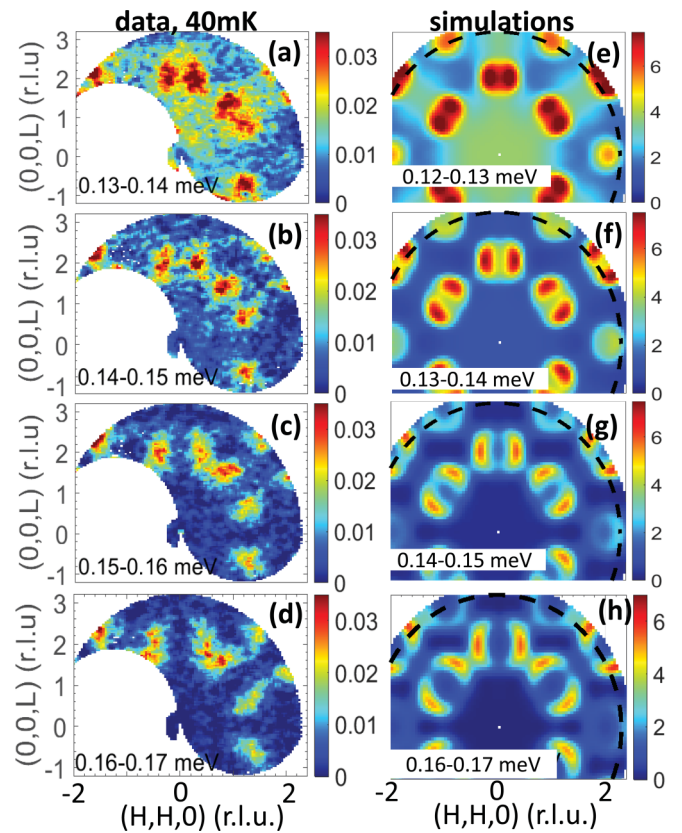

FIG. 4. Wave-vector maps at constant energy comparing the experimental and theoretical spectrum. (a)–(d) show the INS measurement at 40 mK in the $[H, H, L]$ plane integrated over the specified energy ranges. The data were normalized, background subtracted, and integrated over the out-of-plane wave vector by ± 0.15 r.l.u. (e)–(h) show the corresponding neutron scattering structure factor simulated for H_{XYZ}^{DO} [Eq. (1)] using linear spin-wave theory [34] for the same wave-vector integration. For better correspondence with the experiment, the energy integration is systematically shifted downwards by 0.01 meV which is within the limit of the error bars of the exchange interactions.

pinch point wave vector. A schematic of the pinch point and half-moon modes which illustrates their energies and intensity distribution is given in Fig. 1(a).

The half-moon mode in $Nd_2Hf_2O_7$ can be seen in Fig. 3 dispersing out of (0,0,2) which has a high intensity along the transverse $(H, H, 2)$ direction [Fig. 3(a)], but no intensity along the longitudinal $(0, 0, L)$ direction of the traditional pinch point [Fig. 3(b)]. The half-moons shown in Fig. 4, which are observed when taking constant-energy slices through this dispersing mode, are due to its highly directional intensity distribution. Integrating over the dispersing half-moon mode reveals its rotated pinch point pattern with opposite intensity distribution to that of the flat pinch point mode [compare Figs. 2(a) and 2(b)].

To conclude, we have investigated the magnetic properties of $Nd_2Hf_2O_7$ and found it to separate into distinct uncoupled divergence-free and divergence-full parts which give rise to separate features. Long-range AIAO spin order (divergence full) coexists with a dynamic Coulomb phase characterized by 2I2O fluctuations observed as a flat, gapped, pinch point

mode (divergence free). Additional dispersive excitations (divergence full) are observed at high energies which touch the flat mode at the pinch points. We have performed a detailed experimental investigation along with spin-wave calculations of the high energy excitations. Our results confirm recent theories that predict that these modes also host a pinch point pattern perpendicular to the conventional pinch point direction with the opposite intensity distribution [27,28]. Because of the dispersing nature of this pinch point pattern, it is observed as half-moons in constant energy slices through the INS data, very different from the uniform rings observed for conventional spin waves. Half-moons therefore

signal proximity to a Coulomb phase where violation of spin-ice rules allows a divergence-full part to exist that forms a dispersive pinch point pattern in its own right corresponding to monopole propagation.

[1] C. L. Henley, Annu. Rev. Condens. Matter Phys. **1**, 179 (2010).

[2] S. T. Bramwell and M. J. P. Gingras, Science **294**, 1495 (2001).

[3] T. Fennell, P. P. Deen, A. R. Wildes, K. Schmalzl, D. Prabhakaran, A. T. Boothroyd, R. J. Aldus, D. F. McMorrow, and S. T. Bramwell, Science **326**, 415 (2009).

[4] D. J. P. Morris, D. A. Tennant, S. A. Grigera, B. Klemke, C. Castelnovo, R. Moessner, C. Czternasty, M. Meissner, K. C. Rule, J.-U. Hoffmann, K. Kiefer, S. Gerischer, D. Slobinsky, and R. S. Perry, Science **326**, 411 (2009).

[5] B. C. den Hertog and M. J. P. Gingras, Phys. Rev. Lett. **84**, 3430 (2000).

[6] C. Castelnovo, R. Moessner, and S. L. Sondhi, Nature (London) **451**, 42 (2008).

[7] M. Hermele, M. P. A. Fisher, and L. Balents, Phys. Rev. B **69**, 064404 (2004).

[8] N. Shannon, O. Sikora, F. Pollmann, K. Penc, and P. Fulde, Phys. Rev. Lett. **108**, 067204 (2012).

[9] O. Benton, O. Sikora, and N. Shannon, Phys. Rev. B **86**, 075154 (2012).

[10] M. E. Brooks-Bartlett, S. T. Banks, L. D. C. Jaubert, A. Harman-Clarke, and P. C. W. Holdsworth, Phys. Rev. X **4**, 011007 (2014).

[11] J. Xu, V. K. Anand, A. K. Bera, M. Frontzek, D. L. Abernathy, N. Casati, K. Siemensmeyer, and B. Lake, Phys. Rev. B **92**, 224430 (2015).

[12] E. Lhotel, S. Petit, S. Guitteny, O. Florea, M. Ciomaga Hatnean, C. Colin, E. Ressouche, M. R. Lees, and G. Balakrishnan, Phys. Rev. Lett. **115**, 197202 (2015).

[13] J. Xu, C. Balz, C. Baines, H. Luetkens, and B. Lake, Phys. Rev. B **94**, 064425 (2016).

[14] S. Petit, E. Lhotel, B. Canals, M. Ciomaga Hatnean, J. Ollivier, H. Mutka, E. Ressouche, A. R. Wildes, M. R. Lees, and G. Balakrishnan, Nat. Phys. **12**, 746 (2016).

[15] J. Xu, O. Benton, V. K. Anand, A. T. M. N. Islam, T. Guidi, G. Ehlers, E. Feng, Y. Su, A. Sakai, P. Gegenwart, and B. Lake, Phys. Rev. B **99**, 144420 (2019).

[16] E. Lhotel, S. Petit, M. Ciomaga Hatnean, J. Ollivier, H. Mutka, E. Ressouche, M. R. Lees, and G. Balakrishnan, Nat. Commun. **9**, 3786 (2018).

[17] J. Xu, A. T. M. N. Islam, I. N. Glavatskyy, M. Reehuis, J.-U. Hoffmann, and B. Lake, Phys. Rev. B **98**, 060408(R) (2018).

[18] L. Opherden, J. Hornung, T. Herrmannsdörfer, J. Xu, A. T. M. N. Islam, B. Lake, and J. Wosnitza, Phys. Rev. B **95**, 184418 (2017).

[19] S. Guitteny, J. Robert, P. Bonville, J. Ollivier, C. Decorse, P. Steffens, M. Boehm, H. Mutka, I. Mirebeau, and S. Petit, Phys. Rev. Lett. **111**, 087201 (2013).

[20] T. Fennell, M. Kenzelmann, B. Roessli, H. Mutka, J. Ollivier, M. Ruminy, U. Stuhr, O. Zaharko, L. Bovo, A. Cervellino, M. K. Haas, and R. J. Cava, Phys. Rev. Lett. **112**, 017203 (2014).

[21] M. Taillefumier, J. Robert, C. L. Henley, R. Moessner, and B. Canals, Phys. Rev. B **90**, 064419 (2014).

[22] J. Robert, B. Canals, V. Simonet, and R. Ballou, Phys. Rev. Lett. **101**, 117207 (2008).

[23] J. G. Rau and M. J. P. Gingras, Nat. Commun. **7**, 12234 (2016).

[24] M. Udagawa, L. D. C. Jaubert, C. Castelnovo, and R. Moessner, Phys. Rev. B **94**, 104416 (2016).

[25] T. Mizoguchi, L. D. C. Jaubert, and M. Udagawa, Phys. Rev. Lett. **119**, 077207 (2017).

[26] P. Saha, D. Zhang, S.-H. Lee, and G.-W. Chern, Phys. Rev. B **103**, 224402 (2021).

[27] H. Yan, R. Pohle, and N. Shannon, Phys. Rev. B **98**, 140402(R) (2018).

[28] T. Mizoguchi, L. D. C. Jaubert, R. Moessner, and M. Udagawa, Phys. Rev. B **98**, 144446 (2018).

[29] V. K. Anand, D. L. Abernathy, D. T. Adroja, A. D. Hillier, P. K. Biswas, and B. Lake, Phys. Rev. B **95**, 224420 (2017).

[30] V. K. Anand, A. K. Bera, J. Xu, T. Herrmannsdörfer, C. Ritter, and B. Lake, Phys. Rev. B **92**, 184418 (2015).

[31] L. Opherden, T. Bilitewski, J. Hornung, T. Herrmannsdörfer, A. Samartzis, A. T. M. N. Islam, V. K. Anand, B. Lake, R. Moessner, and J. Wosnitza, Phys. Rev. B **98**, 180403(R) (2018).

[32] J. Ollivier and H. Mutka, J. Phys. Soc. Jpn. **80**, SB003 (2011).

[33] R. Ewings, A. Buts, M. Le, J. van Duijn, I. Bustinduy, and T. Perring, Nucl. Instrum. Methods Phys. Res., Sect. A **834**, 132 (2016).

[34] See Supplemental Material at http://link.aps.org/supplemental/10.1103/PhysRevB.106.L100401 for details of the data treatment, spin-wave model, extracted parameters, and higher-temperature data.

[35] Y. Su, K. Nemkovskiy, and S. Demirdiş, J. Large-Scale Res. Facil. **1**, A27 (2015).

[36] O. Benton, Phys. Rev. B **94**, 104430 (2016).

[37] Y.-P. Huang, G. Chen, and M. Hermele, Phys. Rev. Lett. **112**, 167203 (2014).

[38] K. A. Ross, L. Savary, B. D. Gaulin, and L. Balents, Phys. Rev. X **1**, 021002 (2011).

[39] S. Toth and B. Lake, J. Phys.: Condens. Matter **27**, 166002 (2015).

[40] J. Xu, O. Benton, A. T. M. N. Islam, T. Guidi, G. Ehlers, and B. Lake, Phys. Rev. Lett. **124**, 097203 (2020).

[41] M. Léger, E. Lhotel, M. Ciomaga Hatnean, J. Ollivier, A. R. Wildes, S. Raymond, E. Ressouche, G. Balakrishnan, and S. Petit, Phys. Rev. Lett. **126**, 247201 (2021).